GEOPHYSICS, VOL. 85, NO. 1 (JANUARY-FEBRUARY 2020); P. J1–J13, 10 FIGS., 2 TABLES.
10.1190/GEO2018-0851.1

Iterative magnetic forward modeling for high susceptibility based on integral equation and Gauss-fast Fourier transform

Fang Ouyang[1] and Longwei Chen[2]

ABSTRACT

Self-demagnetization due to strongly magnetic bodies can seriously affect the interpretation of magnetic anomalies. Conventional numerical methods often neglect the self-demagnetization effects and limit their use to low susceptibilities ($\chi < 1$ SI). We have developed a novel iterative method based on the integral equation and the Gauss-fast Fourier transform (FFT) technique for calculating the magnetic field from finite bodies of high magnetic susceptibility and arbitrary shapes. The method uses a segmented model consisting of prismatic voxels to approximate a complex target region. In each voxel, the magnetization is assumed to be constant, so that the integral equation in the spatial domain can reduce to a simple form with lots of merit in numerical calculation after the 2D Fourier transform. Moreover, a contraction operator is derived to ensure the convergence of the iterative calculation, and the Gauss-FFT technique is applied to reduce numerical errors due to edge effects. Our modeling results indicate that this new iterative scheme performs well in a wide range of magnetic susceptibilities (1–1000 SI). For lower susceptibilities ($\chi \leq 10$ SI), the iterative algorithm converges rapidly and indicates very good correlation with the analytical solutions. At higher susceptibilities ($10 < \chi \leq 100$ SI), our method still performs well, but the numerical accuracy improves with a relatively slow speed. In the extreme case ($\chi = 1000$ SI), an acceptable result is also obtained after sufficient iterative computation. A further improvement in the numerical precision can be achieved by increasing the number of prismatic voxels, but at the same time, the computational time increases linearly with the size of the voxels.

INTRODUCTION

Self-demagnetization effects due to strongly magnetic bodies have received considerable attention for many years; recently, there has been an upsurge in interest in the topic. Much of the interest is driven by the fact that the magnetic data obtained from mineral deposits with high susceptibilities under complicated geologic conditions are always spurious. This leads to significant challenges in the interpretation of a magnetic survey. The major cause of the problem is the surface divergence of magnetic poles that gives rise to a self-demagnetizing field inside the magnetic bodies with high magnetic susceptibilities (Telford et al., 1990; Guo et al., 2001; Purss and Cull, 2005). This demagnetizing field approximately opposes the external magnetic field in direction. As a result, the magnitude and direction of the resultant magnetic field are altered.

For magnetic bodies with regular shapes, such as prisms, cylinders, spheres, and ellipsoids, analytical solutions are available in magnetic forward calculation (Gay, 1963; Bhattacharyya, 1964; Hjelt, 1972; Emerson et al., 1985; Clark et al., 1986; Kaufman, 1992; Blakely, 1996). However, in more general cases, it is often difficult to obtain the closed-form analytical expressions. One of the most common ways to calculate the magnetic field is to divide the source body into several regular voxels with simple geometry, which permits derivation of analytical expressions for the magnetic field, and then sum up the magnetic response generated by each voxel to approximate the total magnetic anomalies. This approach performs well at low susceptibilities ($\chi < 1$ SI) at which the effects of self-demagnetization are negligible. Practically, most existing methods always ignore the self-demagnetization effect of a rock body while computing its magnetic anomaly (Bott, 1963; Talwani, 1965; Bhattacharyya and Chan, 1977; Ku, 1977). At higher magnetic susceptibilities, however, the conventional numerical calculation is no longer valid and may lead to large approximation errors.

Manuscript received by the Editor 17 December 2018; revised manuscript received 4 August 2019; published ahead of production 07 October 2020; published online 22 November 2019.
[1]China University of Petroleum-Beijing, College of Geophysics and Information Engineering, Beijing, China. E-mail: fangouyang92@163.org.
[2]Guilin University of Technology, School of Earth Sciences, Guilin, China. E-mail: longweichen_glut@glut.edu.cn (corresponding author).

The self-demagnetization becomes quite significant and must be considered (Guo et al., 2001).

Because the magnetic field due to strongly magnetic bodies is seriously affected by self-demagnetization, magnetic forward modeling becomes much more difficult in this case. To solve the field problems, various spatial-domain numerical methods have been developed during the past few decades. Sharma (1966, 1968) presents an integral equation method to compute the magnetic anomalies and demagnetization effect caused by a finite body of arbitrary shape. He represents the magnetized body by rectangular prisms and reduces the volume integral equation of the problem into a set of linear algebraic equations by means of the method of subvolumes. Eskola and Tervo (1980) and Lee (1980) represent the magnetic field due to a body in terms of various field components over its surface. However, these methods perform poorly for bodies whose boundaries are not smooth. Furness (1999) provides an improved alternative technique. He implements the integral equation solution provided by Phillips (1934) to the general 3D geophysical magnetic problem and successfully improves the stability of the method. Lelievre and Oldenburg (2006) develop a full solution to Maxwell's equations for source-free magnetostatics using a finite-volume discretization. Purss and Cull (2005) calculate the magnetic field due to magnetic bodies with high magnetic susceptibility on an iteration-by-iteration basis through a segmented model defined by spherical voxels of uniform arbitrary diameter. Significant work related to self-demagnetization has also been published in the detection and discrimination of the unexploded ordnance (Butler et al., 2003; Zhang et al., 2003; Billings, 2004; Sanchez et al., 2008). A criticism of all these spatial-domain methods is that there can be a dramatic increase in computation time when the target region is large and complicated, especially for 3D forward problems based on the volume integral equation.

To improve computational efficiency, Bhattacharyya and Navolio (1976) propose a frequency-domain approach for calculating magnetic anomalies due to bodies of given shapes. By using the fast Fourier transform (FFT), the magnetic forward modeling based on frequency-domain expressions for the Green's function is found to be computationally very fast. In their work, however, only bodies with low susceptibilities are considered. Moreover, although the adaptation of FFT technique can substantially speed up the calculation of magnetic anomalies, the inherent defects stemming from the discretization of the continuous Fourier transform bring about severe problems, such as edge effects and the resulting "ghost source effect" (Boyd et al., 2001; Wu and Tian, 2014). To reduce the negative influence of the FFT technique on numerical results, grid expansion is the simplest strategy (Tontini et al., 2009). Recently, Wu and Tian (2014) propose a new Gauss-FFT method on the basis of a shift sampling scheme developed by Chai and Hinze (1988) to improve the computational accuracy and to avoid truncation effects due to the standard FFT. This method has been successfully applied in magnetic and gravity forward problems (Wu, 2016; Wu and Chen, 2016). However, their work related to magnetic modeling also takes no account of self-demagnetization effects.

In the present work, we aim to develop a novel iterative method based on the integral equation and the 2D Gauss-FFT technique to calculate magnetic anomalies associated with strongly magnetic bodies. The new iterative method uses a segmented model defined by prismatic voxels of arbitrary height and uniform length and width that allow for bodies of complex geometry and high susceptibility in a very convenient way. The whole target area is regarded as the source region, and each voxel with homogeneous magnetization is an elementary source. Then, the magnetic fields due to the elementary sources are expressed as a convolution of the Green's function and the magnetization. This function holds the same form for all voxels, so that the total magnetic field can be approximated by the sum of the elementary fields. By taking the 2D Fourier transform of the total magnetic field, the volume integral equation in the spatial domain can reduce to a simple form with lots of merit in numerical calculation in the Fourier domain. Moreover, to make the iterative calculation convergent, a new contraction operator is derived using the method proposed by Zhdanov and Fang (1997).

This paper is structured as follows. First, we give a concise review of the integral equation, and we derive the contraction operator for iterative calculation. Second, the new iterative scheme for finite magnetic bodies of high susceptibility and arbitrary shapes is described in detail. Finally, the validation of the iterative method is achieved by several models, and then the convergence and accuracy of the new technique are discussed.

THEORY

The magnetization $\mathbf{M}$ due to a volume of magnetic material in the presence of an inducing field $\mathbf{H}$ is (Lelievre and Oldenburg, 2006)

$$\mathbf{M} = \chi\mathbf{H} = \chi(\mathbf{H}_0 + \mathbf{H}_a), \tag{1}$$

where χ is the magnetic susceptibility, $\mathbf{H}_0$ is the background magnetic field, such as the earth's magnetic field (EMF), and $\mathbf{H}_a$ is the anomalous field associated with magnetic material in the region. In most cases, anomalous magnetic fields are often assumed to be negligible and the magnetization reduces to $\mathbf{M} = \chi\mathbf{H}_0$. However, this assumption is valid only for low magnetic susceptibilities ($\chi < 1$ SI). At larger susceptibilities, the magnetic field becomes seriously affected by the induced magnetization in neighboring material. Within the magnetic body, the induced magnetic field is approximately opposite in direction to the background magnetic field, which consequently results in a decrease in $\mathbf{H}$. This phenomenon is called self-demagnetization. Demagnetization plays an important role in calculating magnetic fields due to strongly magnetic bodies and must be taken into consideration.

The integral equation

To make the presentation clear, we first give a concise review of the vector integral equation for the magnetic field. Consider a 3D model with local inhomogeneity V' with an arbitrary varying susceptibility χ. The scalar magnetic potential at point $\mathbf{r}$ in this model can be presented as a sum of background (normal) and anomalous potential,

$$U(\mathbf{r}) = U_0(\mathbf{r}) + U_a(\mathbf{r}), \tag{2}$$

where the background magnetic potential is associated with the EMF, and the anomalous magnetic potential is caused by the anomalous susceptibility distribution, which is given by (Butler et al., 2001)

$$U_a(\mathbf{r}) = -\iiint_{V'} \nabla G(\mathbf{r},\mathbf{r}') \cdot \mathbf{M}(\mathbf{r}')\mathrm{d}V', \tag{3}$$

where $G(\mathbf{r},\mathbf{r}') = 1/(4\pi|\mathbf{r}-\mathbf{r}'|)$ is the scalar Green's function. It can be found as the solution of the following differential equation (Furness, 1999):

$$\nabla^2 G(\mathbf{r},\mathbf{r}') = -\delta(\mathbf{r}-\mathbf{r}'), \tag{4}$$

where δ is the Dirac delta function and $\mathbf{r}'$ is the source point in inhomogeneous domain V'. The magnetic field at point $\mathbf{r}$ is then given by

$$\mathbf{H}(\mathbf{r}) = -\nabla U(\mathbf{r}). \tag{5}$$

In geophysical applications, interest always focuses on the magnetic field. By taking the gradient of equation 3, we conveniently obtain

$$\mathbf{H}_a(\mathbf{r}) = \iiint_{V'} \nabla\nabla G(\mathbf{r},\mathbf{r}') \cdot \mathbf{M}(\mathbf{r}')\mathrm{d}V'. \tag{6}$$

Furthermore, we can also represent the integral equation with respect to the total magnetic field:

$$\mathbf{H}(\mathbf{r}) = \mathbf{H}_0(\mathbf{r}) + \iiint_{V'} \nabla\nabla G(\mathbf{r},\mathbf{r}') \cdot [\chi(\mathbf{r}')\mathbf{H}(\mathbf{r}')]\mathrm{d}V'. \tag{7}$$

For low magnetic susceptibilities, the anomalous magnetic field is negligible compared to the background field, and the magnetization is $\mathbf{M} = \chi\mathbf{H}_0$, so that accurate results can be obtained by direct methods. At higher susceptibilities, however, the demagnetization effects must be considered, and the integral equation should be solved by an iterative procedure. Once the unknown magnetic field is found inside V', we use equation 6 to find the response of the anomaly at any observation position $\mathbf{r}$. The main effort in this paper is devoted to the accurate solution of this problem.

Iterative solver with contraction operator

To solve equation 7, we propose an iterative method with a new contraction operator that assures the convergence of iteration. In this section, we follow Zhdanov and Fang (1997) and derive the new contraction operator for magnetic forward modeling with high susceptibility. For convenience, we rewrite equation 7 using operator notation as

$$\mathbf{H} = \mathbf{H}_0 + \mathbf{H}_a = \mathbf{H}_0 + G_c(\chi\mathbf{H}) = \mathbf{H}_0 + G_c(\mathbf{M}), \tag{8}$$

where G_c is a linear integral operator defined by

$$G_c(\cdot) = \iiint_{V'} \nabla\nabla G(\mathbf{r},\mathbf{r}') \cdot (\cdot)\mathrm{d}V'. \tag{9}$$

In theory, equation 8 can be solved via the method of successive iterations. To guarantee the calculation converge, the operator G_c must be a contraction operator. In other words, the ℓ_2-norm of G_c should be less than one, namely, $\|G_c\| < 1$. However, in practice, this condition does not hold because in general cases, the ℓ_2-norm of the Green's operator is bigger than 1. Using an energy inequality, Zhdanov and Fang (1997) construct a globally convergent modified Born series expansion for 3D electromagnetic modeling. Here, we will follow their method and use a linear transformation to transform the operator G_c into a new operator G_c^m, the norm of which is always less than one.

As mentioned above, for a strongly magnetic body, the demagnetizing field within it is approximately opposite in direction to the external field. Therefore, an important inequality can be obtained:

$$\sqrt{\iiint_{V'} \left|\mathbf{H}_a + \frac{\mathbf{M}}{2}\right|^2 \mathrm{d}V'} \le \sqrt{\iiint_{V'} \left|\frac{\mathbf{M}}{2}\right|^2 \mathrm{d}V'}. \tag{10}$$

By making use of equation 8, we have

$$\mathbf{H}_a + \frac{\mathbf{M}}{2} = G_c\left(2\frac{\mathbf{M}}{2}\right) + \frac{\mathbf{M}}{2} = G_c^m\left(\frac{\mathbf{M}}{2}\right), \tag{11}$$

where G_c^m is the new operator that can be applied to any vector-valued function and is given by

$$G_c^m(\mathbf{x}) = G_c(2\mathbf{x}) + \mathbf{x}. \tag{12}$$

Substitution of equation 12 into equation 10 gives the following inequality for the operator G_c^m:

$$\|G_c^m(\mathbf{x})\| \le \|\mathbf{x}\|, \tag{13}$$

where $\|\cdot\| = \sqrt{\iiint_{V'} |\cdot|^2 \mathrm{d}V'}$ denotes the ℓ^2-norm in a Hilbert space. Using equations 8 and 11, and after some manipulations, we obtain

$$\begin{aligned} \mathbf{H}' &= \mathbf{H}_0 + G_c^m\left(\frac{\chi}{2+\chi}\mathbf{H}'\right) = \mathbf{H}_0 + O_c^m(\mathbf{H}'), \\ \mathbf{H} &= \left(1+\frac{\chi}{2}\right)^{-1}\mathbf{H}'. \end{aligned} \tag{14}$$

According to the Cauchy-Schwartz inequality, equation 13 and $\|\chi/(2+\chi)\|_\infty < 1$ guarantee that the operator O_c^m be contractive, namely,

$$O_c^m(\mathbf{x}) \le \|\chi/(2+\chi)\|_\infty \|G_c^m\| \|\mathbf{x}\| < 1 \cdot \|\mathbf{x}\|. \tag{15}$$

This new contraction operator has advantages over other operators in making the method of successive iterations always convergent.

Equation 14 eventually leads to a new integral equation:

$$\mathbf{H} = \frac{2[G_c(\chi\mathbf{H}) + \mathbf{H}_0] + \chi\mathbf{H}}{2+\chi} = \frac{2(\mathbf{H}_a + \mathbf{H}_0) + \chi\mathbf{H}}{2+\chi}. \tag{16}$$

We note that the contraction of the new integral equation 16 is assured by the inequality 15. In the following magnetic forward modeling, we use equation 16 as an iterative solver to ensure the convergence of our proposed method.

ITERATIVE SCHEME

Now, we discuss the basic principles of the new iterative method of calculating the magnetic field due to strongly magnetic bodies with arbitrary shapes. In general, this iterative method consists of two main parts: the computation of the anomalous magnetic field (equation 6 or the second term on the right side of equation 7 in the Fourier domain in each iteration) and the iterative calculation of the total magnetic field using the contraction operator. The workflow of our iterative algorithm is shown in Figure 1.

Iterative procedure

The various steps of calculation can be described in a simple fashion (Figure 1). First, the model domain is represented by a suitable combination of prismatic voxels ($N_x \times N_y \times N_z$) within which the magnetic susceptibility and the magnetic field are homogeneous. The initial value of the magnetic field in each prism is taken to be equal to the EMF $\mathbf{H}_0$; i.e.,

$$\mathbf{H}^{(i=0)}(x_j, y_m, z_n) = \mathbf{H}_0(x_j, y_m, z_n),$$
$$(1 \le j \le N_x, 1 \le m \le N_y, 1 \le n \le N_z), \qquad (17)$$

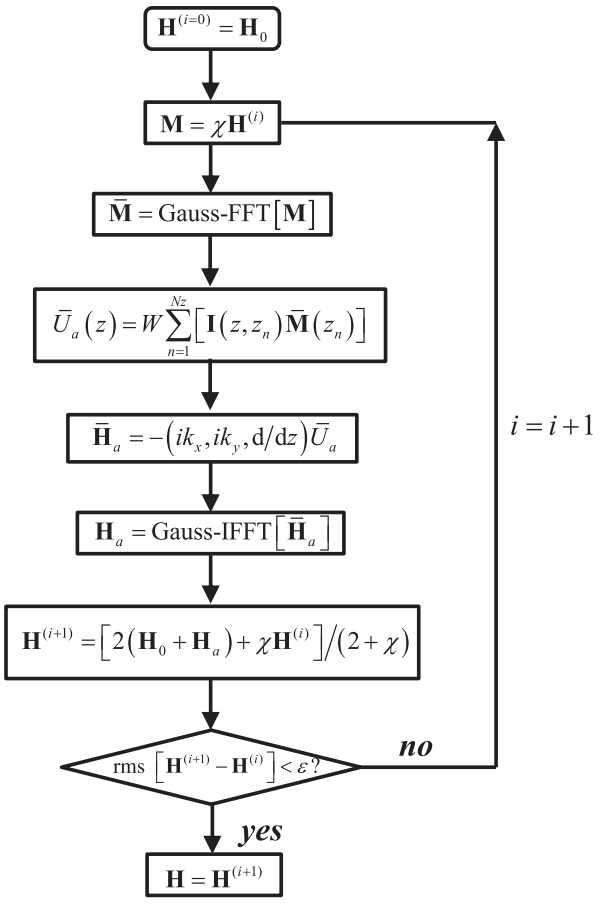

Figure 1. Flow diagram of the novel iterative algorithm for modeling a magnetic field associated with 3D magnetic bodies with high susceptibility.

where the superscript i denotes the ith iteration, $i = 0$ means the initial (0th) iteration, and (x_j, y_m, z_n) denotes the geometric center of the prism or the source point. We note that the observation points align with the center of the model mesh; i.e., $(x, y, z) = (x_j, y_m, z_n)$.

Second, the anomalous magnetic field (equation 6) is calculated in the Fourier domian (k_x, k_y, z):

$$\bar{H}_{ax}(k_x, k_y, z) = -ik_x\bar{U}_a(k_x, k_y, z),$$
$$\bar{H}_{ay}(k_x, k_y, z) = -ik_y\bar{U}_a(k_x, k_y, z),$$
$$\bar{H}_{az}(k_x, k_y, z) = -\frac{\mathrm{d}}{\mathrm{d}z}\bar{U}_a(k_x, k_y, z), \qquad (18)$$

with

$$\bar{U}_a(k_x, k_y, z) = W(k_x, k_y)\sum_{n=1}^{N_z}[\mathbf{I}(k_x, k_y, z, z_n) \cdot \bar{\mathbf{M}}(k_x, k_y, z_n)], \qquad (19)$$

where $\bar{U}_a$ is the 2D Fourier transform of the scalar anomalous magnetic potential U_a. A detailed derivation of equation 19 is provided in Appendix A, and the expressions for W and $\mathbf{I}$ can be found in equations A-4–A-11. In equation 19, $\bar{\mathbf{M}}(k_x, k_y, z_n)$ is obtained by taking the 2D Fourier transform of $\mathbf{M}$, which can be calculated by substituting equation 17 into equation 1; i.e.,

$$\bar{\mathbf{M}}(k_x, k_y, z_n) = \mathrm{FT}[\mathbf{M}(x_j, y_m, z_n)]$$
$$= \mathrm{FT}[\chi(x_j, y_m, z_n)\mathbf{H}^{(i)}(x_j, y_m, z_n)], \qquad (20)$$

where $\chi(x_j, y_m, z_n)$ describes the susceptibility distribution of the model and FT[·] denotes the 2D Fourier transform. Then, the anomalous magnetic field $\mathbf{H}_a$ in the spatial domain can be immediately obtained by taking 2D inverse Fourier transform of equation 18.

For magnetic bodies with low susceptibility, accurate results are reached after the first pass through this process, and the computation can be finished here. For the calculation of the magnetic field due to strongly magnetic bodies, however, an iterative calculation is required. To ensure the convergence of the new iterative method, we adopt the contraction integral equation given in equation 16. Its discrete form is

$$\mathbf{H}^{(i+1)}(x_j, y_m, z_n) = \frac{2[\mathbf{H}_0(x_j, y_m, z_n) + \mathbf{H}_a(x_j, y_m, z_n)] + \chi(x_j, y_m, z_n)\mathbf{H}^{(i)}(x_j, y_m, z_n)}{2 + \chi(x_j, y_m, z_n)}. \qquad (21)$$

In our iterative algorithm, the root mean square (rms) difference is used for the convergence criterion, which is defined as

$$\mathrm{rms}[\mathbf{H}^{(i+1)} - \mathbf{H}^{(i)}] = \sqrt{\frac{\sum_{j,m,n}[\mathbf{H}^{(i+1)}(x_j, y_m, z_n) - \mathbf{H}^{(i)}(x_j, y_m, z_n)]^2}{N_x N_y N_z}} \times 100\%. \qquad (22)$$

If the rms difference between $\mathbf{H}^{(i+1)}$ and $\mathbf{H}^{(i)}$ is less than the required convergence accuracy, the calculation is complete. If not,

assign the value of $\mathbf{H}^{(i+1)}$ to $\mathbf{H}^{(i)}$ and repeat the previous steps until a satisfying result is reached.

Gauss-FFT technique

The 2D Fourier transforms involved in the equations mentioned above are achieved by the Gauss-FFT technique in our algorithm. Although the standard FFT method has been widely applied in numerical computation involved in many geophysical problems, it always suffers from severe edge effects due to discretization and truncation. Therefore, to avoid these problems, we apply the Gauss-FFT technique proposed by Wu and Tian (2014) to our numerical calculation. This technique is based on a combined use of the shift-sampling technique and Gaussian quadrature theory. It has significant advantages over the standard FFT in reducing the truncation effects without grid expansion. Here, we just use the Gauss-FFT technique, and a detailed derivation of the transforms can be found in Wu and Tian (2014) and Zhao et al. (2018).

Following the Gauss-FFT theory, the discrete forms for the 2D Fourier transform can be expressed as

$$\bar{f}(k_x,k_y)=\Delta x\Delta y\sum_{j=0}^{N_x-1}\sum_{m=0}^{N_y-1}f(x_j,y_m)e^{-i(k_xx_j+k_yy_m)},$$
$$f(x_j,y_m)=\frac{1}{\Delta x\Delta y N_xN_y}\sum_I\sum_J\gamma_I\gamma_J\sum_p\sum_q\bar{f}(k_x,k_y)e^{i(k_xx_j+k_yy_m)}, \tag{23}$$

where $k_x=k_{xp}+t_I\Delta k_x$, $k_y=k_{yq}+t_J\Delta k_y$, $\gamma_{I,J}$ is the weighed coefficient, $t_{I,J}$ is the Gaussian node, x and y are the location of equal-spaced points, and k_{xp} and k_{yq} are the wavenumber given by Chen et al. (2016):

$$k_{xp}=p\Delta k_x,\quad \Delta k_x=\frac{2\pi}{N_x\Delta x},\quad p=-\frac{N_x}{2},\quad -\frac{N_x}{2}+1,\cdots,\quad \frac{N_x}{2}-1,$$
$$k_{yq}=q\Delta k_y,\quad \Delta k_y=\frac{2\pi}{N_y\Delta y},\quad q=-\frac{N_y}{2},\quad -\frac{N_y}{2}+1,\cdots,\quad \frac{N_y}{2}-1, \tag{24}$$

where Δx and Δy are the grid sizes in the x- and y-directions. The terms N_x and N_y (even numbers) are the number of discrete points in the two directions.

NUMERICAL EXAMPLES AND DISCUSSIONS

Verification of the iterative method

To verify the computational accuracy of the new iterative algorithm for high magnetic susceptibility, the numerical results are compared with the analytical solutions for three simple models (a sphere with magnetic susceptibility 10 SI, a spherical shell of 100 SI, and a prolate ellipsoid of 10 SI). The analytical solutions for the models are calculated using the formulas derived from Kaufman (1992) (see Appendix B) and the routines provided by Takahashi and Oliveira (2017). The difference between the numerical and analytic result is presented. All examples are calculated by the Gauss-FFT technique with four Gaussian nodes in this paper and are carried out on a personal computer with Intel i7 Core 3.4 GHz and 32 GB RAM.

The model domain extends from 0 to 1000 m in the x-, y-, and z-directions, respectively, and it consists of $200\times200\times200$ prisms with equal intervals (see Figure 2). The magnetic anomaly is a 3D solid magnetic body of high susceptibility in an inducing field with strength 50,000 nT, inclination 58.3°, and different declination. The value of the background susceptibility is 0 SI. The first model shown in Figure 3 is a magnetic sphere with susceptibility of 10 SI, which is representative of the type of situation encountered in mineral exploration. The radius of the sphere is 200 m, and its center is located at (500 m, 500 m, 500 m), which is in the middle of the target area. The depth of the spherical center to the ground is 500 m. Numerical and analytic results for the magnetic sphere and the difference between them are shown in Figure 4. The second example is a spherical shell with a higher susceptibility of 100 SI. Its inner and outer radius is 150 and 200 m, respectively. Figure 5 presents a

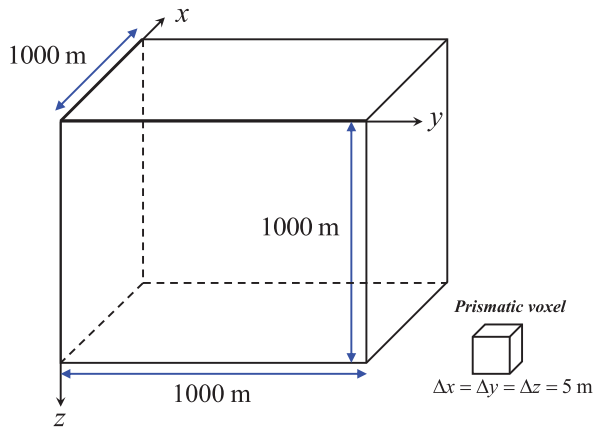

Figure 2. A schematic diagram of the computational region. The whole region is discretized in a grid containing $200\times200\times200$ prismatic voxels with 5 m dimensions. The grid cell is shown on the bottom right corner.

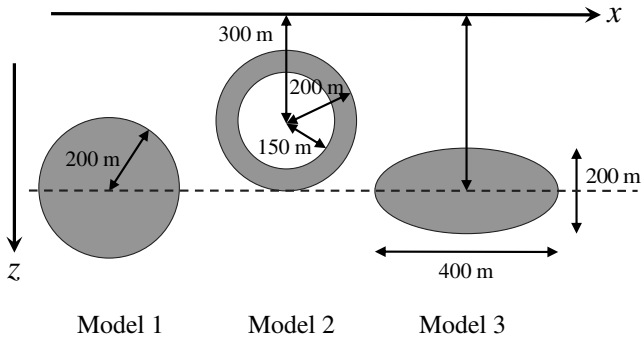

Figure 3. A schematic diagram of the three models introduced for verification of the novel iterative method. The view is a vertical cross section along $y=500$ m. The first model is a solid magnetic sphere with radius 200 m and susceptibility 10 SI; the second model is a magnetic spherical shell with inner radius 150 m, outer radius 200 m, and susceptibility 100 SI; and the third model is a magnetic prolate ellipsoid with horizontal long axes 200 m, short axes 100 m, and susceptibility 10 SI. The geometric centers of the first and third model are located at (500 m, 500 m, 500 m), and the second model is placed at (500 m, 250 m, 300 m).

comparison of the numerical and analytic results. The third model is a prolate ellipsoid with horizontal major axes 200 m, minor axes 100 m, and a susceptibility of 10 SI. Figure 6 shows the modeled response and the differences between the numerical and analytic responses for the spheroid. We also provide the statistical properties of the misfits, including the minimum and maximum values, the rms error, and the relative rms (Rrms) error (Table 1). The Rrms error is computed as (Wu, 2016)

$$\mathrm{Rrms}[H] = \frac{\mathrm{rms}[\hat{H} - H]}{\mathrm{rms}[\hat{H}]} \times 100\%, \tag{25}$$

where H can be any magnetic component calculated by the iterative method and $\hat{H}$ refers to the analytical solution.

All tests show that the numerical results calculated by the new iterative method have a good correlation with the analytical solutions (Figures 4–6). For the sphere of 10 SI, the rms error is 7.75 for B_{ax}, B_{ay} and 10.43 for B_{az} (Table 1). The Rrms error for all the magnetic components is less than 1% (0.71% for B_{ax}, B_{ay} and 0.6% for B_{az}). For the magnetic shell with a higher susceptibility of 100 SI, the Rrms error has a slightly larger value of 1% for all three magnetic components. For the magnetic prolate ellipsoid, the total field in Figure 6 is in close agreement. Moreover, no edge effect is observed in all the examples. This implies that in forward magnetic modeling for high magnetic susceptibility, the Gauss-FFT technique can also effectively avoid the negative effects caused by discretization and truncation commonly occurred in standard FFT. We conclude that the new iterative method based on the integral equation and the Gauss-FFT technique performs well in calculating magnetic field from magnetic bodies with high susceptibility.

Convergence of the iterative method

The convergence behavior of the new iterative technique is closely related to the magnitude of the magnetic susceptibility and the number of prismatic voxels used. To assess and analyze the influence of these factors, the same spherical model mentioned above with different magnetic susceptibilities and grid numbers is considered. For comparison of numerical precision after each iteration, the Rrms difference is used by replacing H in equation 22

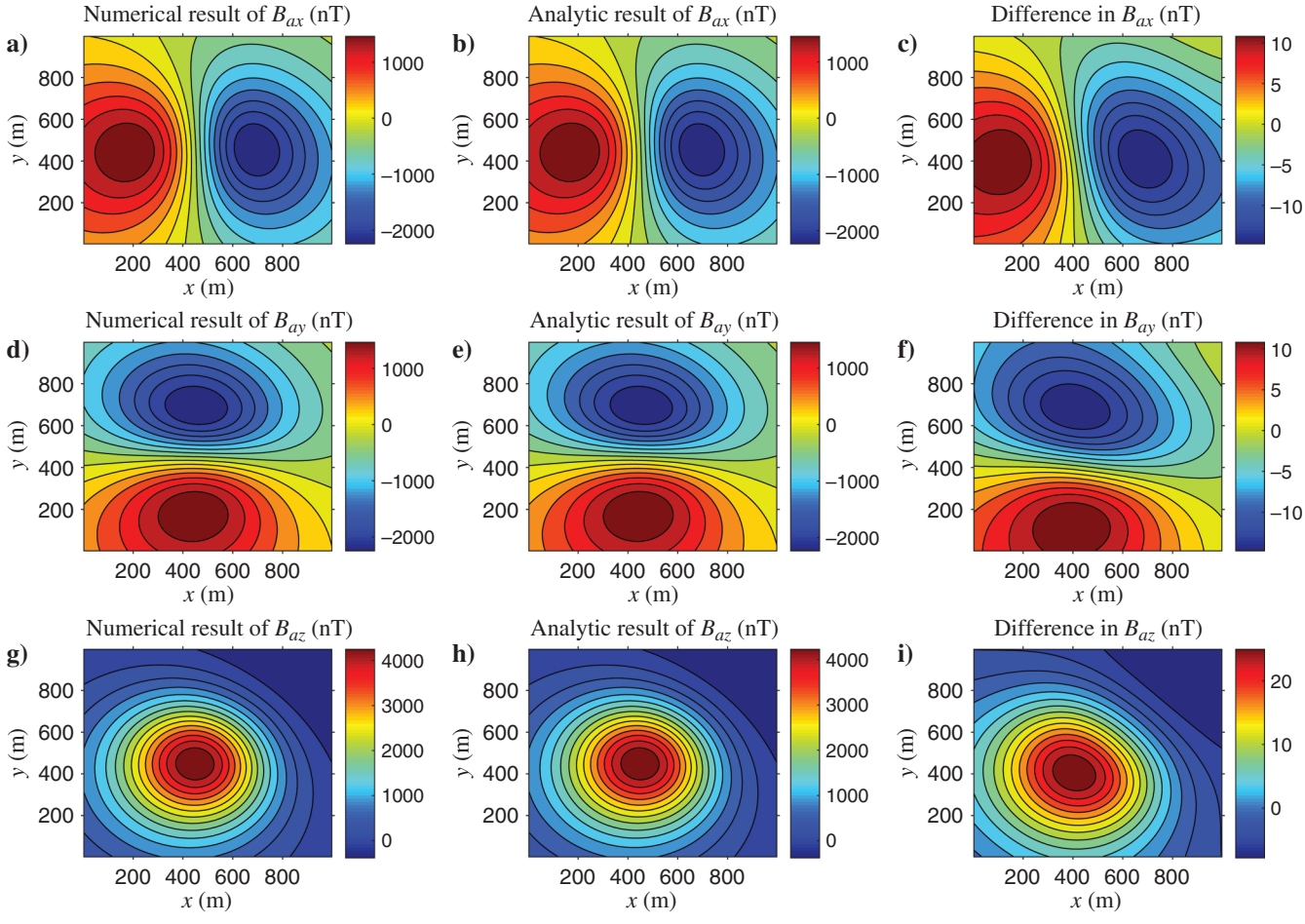

Figure 4. Surface magnetic anomalies due to a magnetic sphere with a susceptibility of 10 SI in an inducing field with strength 50,000 nT, declination 45°, and inclination 58.3°. (a, d, and g) The three anomalous magnetic components (B_{ax}, B_{ay}, and B_{az}) calculated using the proposed iterative method. (b, e, and h) The analytic result calculated by the theoretical formulas provided by Kaufman (1992); the difference between the numerical and analytic result is shown in (c, f, and i).

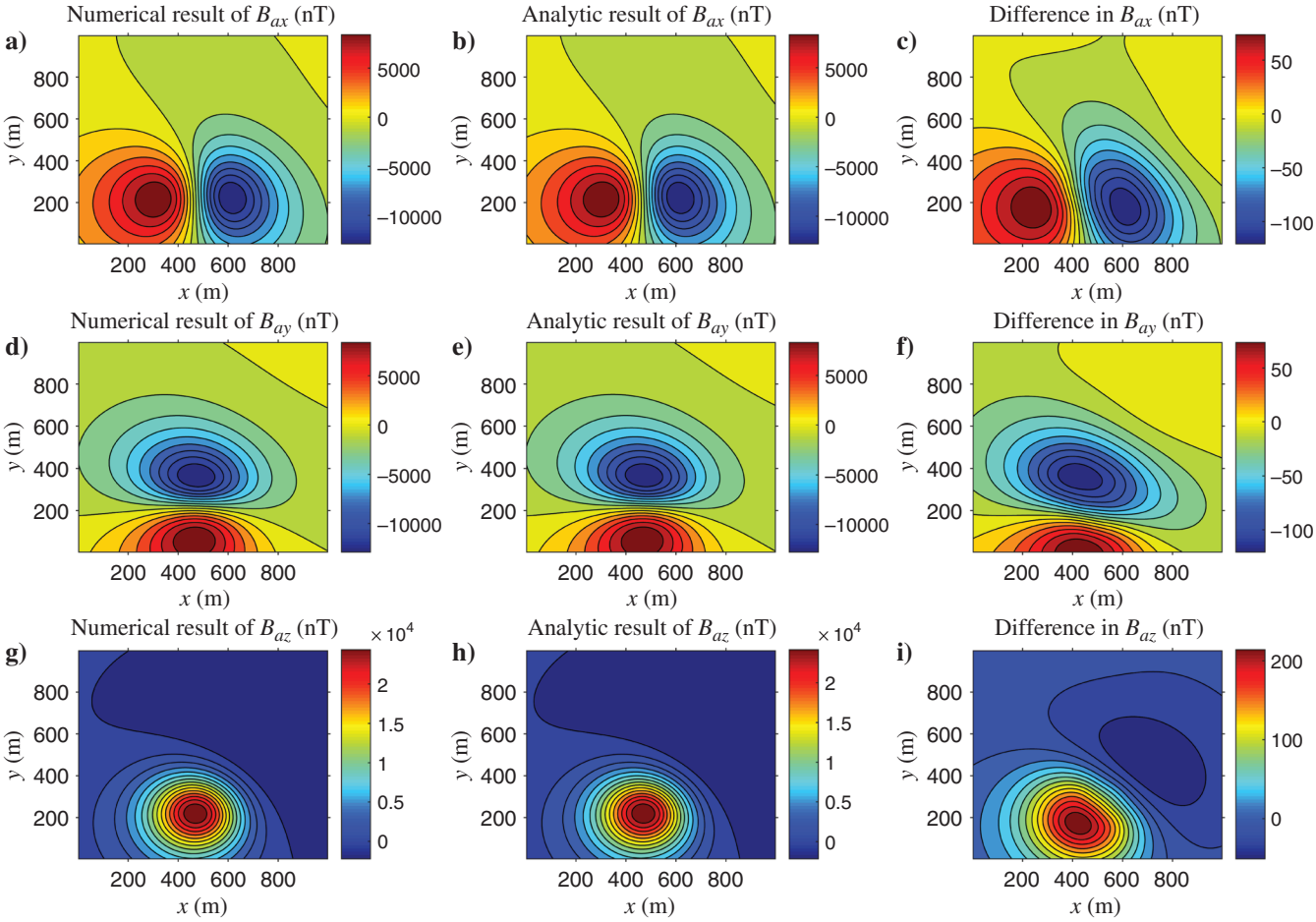

Figure 5. Surface magnetic anomalies due to a magnetic spherical shell with a susceptibility of 100 SI in an inducing field with strength 50,000 nT, declination 45°, and inclination 58.3°. (a, d, and g) The three anomalous magnetic components (B_{ax}, B_{ay}, and B_{az}) calculated using the proposed iterative method. (b, e, and h) The analytic result calculated by the theoretical formulas provided by Kaufman (1992); the difference between the numerical and analytic result is shown in (c, f, and i).

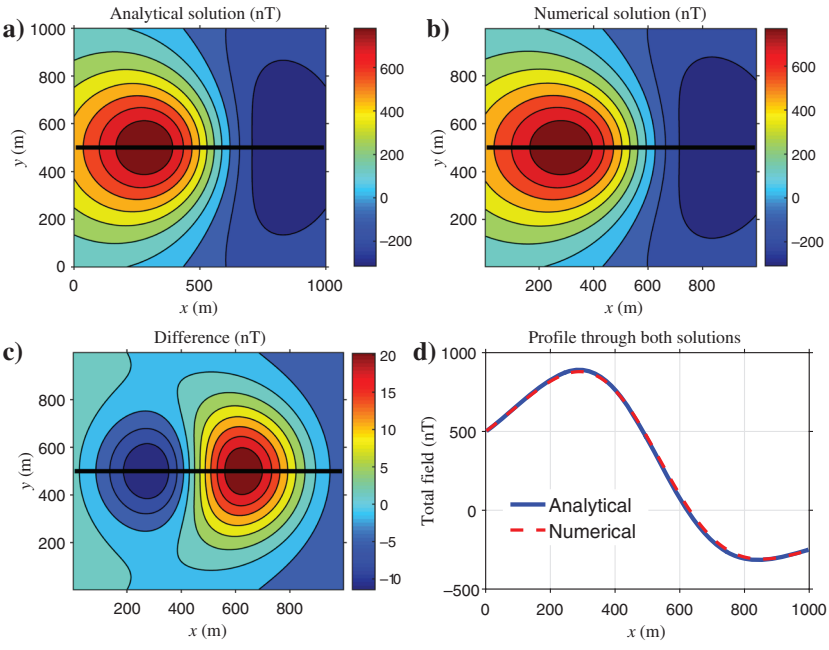

Figure 6. Total-field data maps and profiles for a magnetic spheroid with a susceptibility of 10 SI in an inducing field with strength 50,000 nT, declination 0°, and inclination 58.3°. The spheroid has horizontal long axes with azimuthal angle 0°: (a) analytical solution calculated using the routines provided by Takahashi and Oliveira (2017), (b) numerical solution calculated using the proposed iterative method, (c) difference between the numerical and analytical solution, and (d) profiles through both solutions, which are indicated by the heavy solid lines on the data maps.

with $H^{(i)}$, where $H^{(i)}$ can be any magnetic component calculated after the ith iterations.

The magnetic susceptibility

The magnetic field is mainly controlled by the distribution of magnetic susceptibility beneath the ground. This test compares the Rrms errors in anomalous fields iteratively calculated using the proposed method for different susceptibilities ranging from 1 to 1000 SI. Figure 7 presents the trend of Rrms error versus the number of iterations at different susceptibilities. It is clearly shown that the convergence rate of the new iterative method decreases with the magnetic susceptibility. Moreover, the Rrms difference for the three anomalous magnetic components (B_{ax}, B_{ay}, and B_{az}) changes with the number of iterations in a similar way at each susceptibility. For low magnetic susceptibilities ($\chi \leq 1$ SI), the new iterative method performs very well, and the Rrms errors are approximately 0.1% after the third iterations. At moderate magnetic susceptibilities ($1 < \chi \leq 10$ SI), there is also a good correlation between the modeled results and analytical solutions. The Rrms errors after the fifth iterations are approximately 1%. However, at higher magnetic susceptibilities ($10 < \chi \leq 100$ SI), the convergence of the new iterative method slows down. A maximum Rrms error (approximately 2%) is achieved after nine iterations, and further iterative calculation results in little difference. For high to extreme magnetic susceptibilities ($100 < \chi \leq 1000$ SI), the iterative algorithm converges much more slowly. It seems that the algorithm is still on its way to the convergence limit even after 19 iterations, and only a moderate cor-

Table 1. Statistics of the errors for the three discrete models (sphere, spherical shell, and prolate ellipsoid) using the novel iterative method.

Model		B_{ax}	B_{ay}	B_{az}	Total field
Sphere	Min	−2.2493e + 03	−2.2493e + 03	−3.8838e + 02	−8.0050e + 02
	Max	+1.7127e + 03	+1.7127e + 03	+4.5617e + 03	+3.9747e + 03
	rms	7.7543	7.7543	10.4317	10.2944
	Rrms	0.0071	0.0071	0.0060	0.0067
Spherical shell	Min	−1.2901e + 04	−1.2901e + 04	−2.2248e + 03	−4.5971e + 03
	Max	+9.8011e + 03	+9.8011e + 03	+2.6139e + 04	+2.2773e + 04
	rms	40.7568	38.7544	60.7368	55.6401
	Rrms	0.0101	0.0102	0.0102	0.0103
Prolate ellipsoid	Min	−6.4273e + 02	−4.2833e + 02	−2.0120e + 02	−3.0988e + 02
	Max	+3.4188e + 02	+4.2833e + 02	+1.0338e + 03	+8.7936e + 02
	rms	6.3501	4.0267	9.2433	6.7809
	Rrms	0.0219	0.0176	0.0224	0.0186

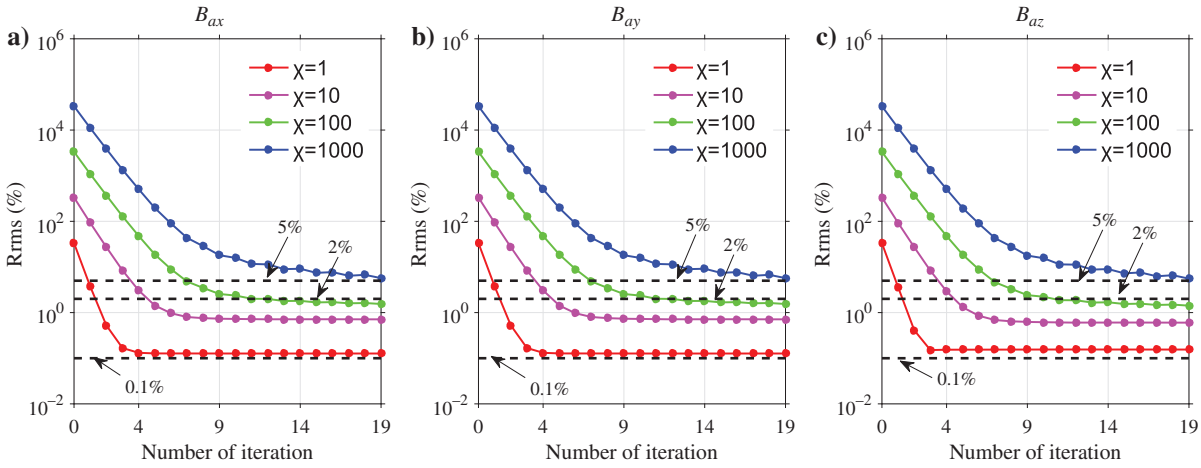

Figure 7. Comparison of the Rrms error in B_{ax}, B_{ay}, and B_{az} calculated using the proposed iterative method versus the number of iterations for each magnetic susceptibility.

relation with the analytical solution occurs after the complete calculation with an Rrms error of 5%. Although further iterations can help to improve the numerical precision, these minor improvements have significant computational cost.

Grid sampling

Grid sampling is the major cause of error in almost all magnetic forward-modeling methods. An increase in the grid number, or a decrease in the size of the prisms, can efficiently reduce the numerical error of the modeled results and also leads to an increase in the calculation time. Therefore, it is important to find a balance between computational accuracy and cost. Here, two cases are discussed to investigate the effects of the grid number. In case 1, we set $N_z = 50$, 100, 150, 200, 300, 400 and $N_x = N_y = 200$ so that the influence of the vertical grids can be analyzed. In case 2, we set $N_x = N_y = 50$, 100, 150, 200, 300, 400 and $N_z = 200$. The latter case is included to illustrate the effects of the number of horizontal grids on the Gauss-FFT. In the new iterative algorithm, the Gauss-FFT technique is taken on a bunch of different horizontal planes, so the computing speed and accuracy of the transform will be significantly affected by the number of the horizontal grids. In both cases, the target magnetic body is a solid magnetic sphere with different susceptibilities (10 and 100 SI).

Figure 8 shows the comparison of the Rrms errors in three magnetic components versus the number of iterations for case 1 at 10 and 100 SI. The convergence of the present numerical solution is illustrated in Figure 9. These figures illustrate that finer vertical grid sampling can to some extent improve the accuracy. The convergence of the algorithm seems to be achieved in a slightly fluctuating way at high susceptibilities (Figure 9d–9f). Moreover, the solutions have essentially converged for a discretization involving 150 vertical grids, and little difference in the profile arises from further increasing the number of N_z to 400. It is also noteworthy that the essential features of the anomaly can be present in the case of the coarsest discretization ($N_z = 50$). In conclusion, three important points can be drawn from these figures: (1) The Rrms errors in three components have a similar trend over the number of iterations, (2) the convergence rate increases with the number of vertical grids, and (3) the computational accuracy can be improved by increasing N_z, but there is a limit in such improvement.

Figure 10 shows a comparison of the Rrms errors in three anomalous magnetic components versus the number of iterations for case 2. The figure illustrates that an acceptable correlation (Rrms less than 2%) between the modeled results and analytical solutions is essentially achieved for the case of $N_x = N_y = 50$ at 10 SI and $N_x = N_y = 120$ at 100 SI. In addition, a further increase in the horizontal grids from 100 to 300 results in little difference in numerical accuracy. This implies that a refinement of the horizontal grids does not definitely give rise to a significant improvement in the numerical accuracy of the 2D Gauss-FFT. Table 2 presents the relevant calculation time for those who are interested in our iterative method. In sum, to ensure an acceptable accuracy and efficiency, it seems that $N_x = N_y = N_z = 150$ is the best choice for the magnetic spherical model with high magnetic susceptibility.

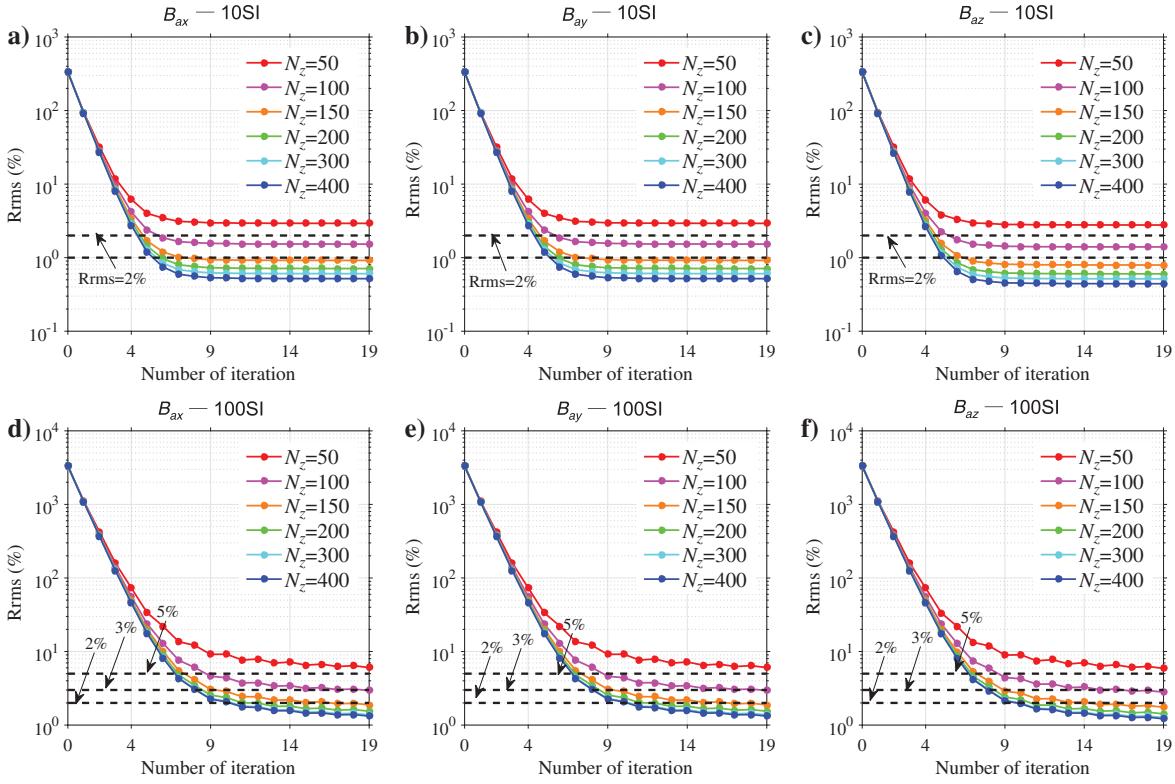

Figure 8. Comparison of the Rrms error in B_{ax}, B_{ay}, and B_{az} calculated using the proposed iterative method versus the number of iterations at 10 and 100 SI for case 1 ($N_x = N_y = 200$).

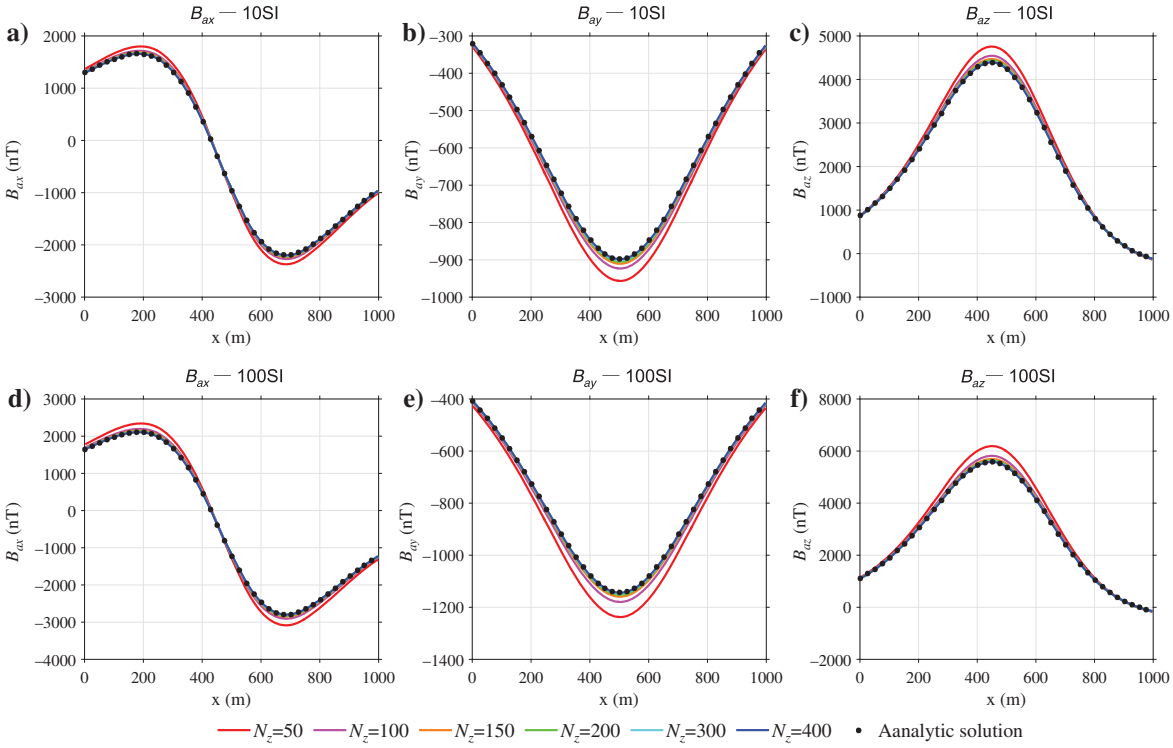

Figure 9. Surface magnetic anomalies along the profile $y = 497.5$ m after 19 iterations calculated using the proposed iterative method for case 1 compared with analytic results at 10 and 100 SI.

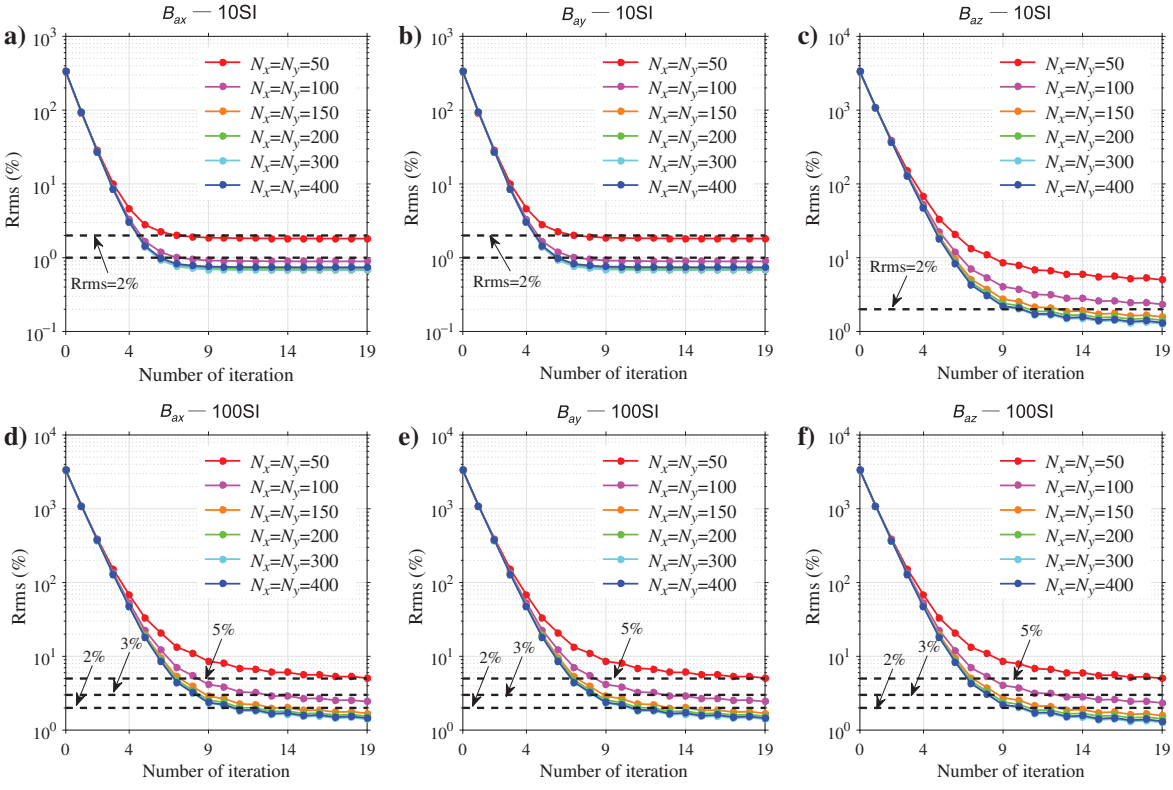

Figure 10. Comparison of the Rrms error in B_{ax}, B_{ay}, and B_{az} calculated using the proposed iterative method versus the number of iterations at 10 and 100 SI for case 2 ($N_z = 200$).

Table 2. Average computation time per iteration for calculating the three magnetic components by the new iterative method. Case 1 is corresponding to the results in Figures 8 and 9, whereas case 2 is corresponding to the results in Figure 10.

Case 1($N_x = N_y = 200$)		Case 2($N_z = 200$)	
N_z	Time consumption (s)	N_x/N_y	Time consumption (s)
50	22.9	50	7.5
100	55.6	100	32.1
150	99.7	120	49.9
200	154.8	150	83.9
300	293.1	200	157.2
400	471.5	300	363.5

CONCLUSION

The new iterative method for high magnetic susceptibility is an accurate spectral solution based on the integral equation and the Gauss-FFT technique. Different from most existing numerical methods for magnetic forward modeling, we deal with the volume integral formula in the Fourier domain, in which the triple integral can be simplified to a simple form that has lots of merit in achieving high numerical accuracy and improving computational efficiency. The use of the prismatic voxel as the volume element can significantly simplify the magnetic forward problems, and it allows more flexibility in the fast computation of the magnetic field. High-accuracy 2D Gauss-FFT technique is incorporated in the presented method to avoid edge effects, and a new contraction operator is applied to make the iterative calculation convergent.

Comparisons of the results calculated by the new iterative method with analytical solutions for models with different magnetic susceptibilities from low to high verify the accuracy of the algorithm. We demonstrate that the new method performs well for a wide range of susceptibilities, from low to high. At lower susceptibilities ($\chi \leq 10$ SI), the calculated results show a very good correlation with analytical solutions and converge very rapidly. As the magnetic susceptibility increases ($10 < \chi \leq 100$ SI), the proposed method still performs well but converges more slowly, and an increased number of iterations is required to meet the expected accuracy. At high to extreme susceptibilities ($100 < \chi \leq 1000$ SI), acceptable results can be obtained by the proposed method after sufficient iterative computation. Further improvement in numerical precision at extreme susceptibilities can be achieved by increasing the number of prisms, but at the cost of additional calculation time.

In summary, the present iterative technique provides an accurate convergence method to model the magnetic field associated with induction in 3D magnetic bodies of high magnetic susceptibility. Moreover, the new method is expected to have good applicability for parallel programming.

ACKNOWLEDGMENTS

The authors are very grateful to reviewers P. Furness, M. Zhdanov, J. Shragge and two anonymous reviewers for their critique, helpful comments, and constructive suggestions that helped to improve the manuscript significantly. This study was funded by the National Natural Science Foundation of China under grant no. 41404106 and the Natural Science Foundation of Guangxi Province of China under grant no. 2018GXNSFBA138049.

DATA AND MATERIALS AVAILABILITY

Data associated with this research are available and can be obtained by contacting the corresponding author.

APPENDIX A

NUMERICAL IMPLEMENTATION

Implementation of the new iterative scheme initially requires the solution of equation 3, more specifically, the anomalous magnetic potential due to strongly magnetic bodies. To solve the problem in an efficient way, we regard the whole computational area as the source region and divide it into $N_x \times N_y \times N_z$ prisms in the x-, y-, and z-directions. For each prism, its geometric center is (x_j, y_m, z_n) with the length of Δx, Δy, and Δz_n along the x-, y-, and z-directions, where the subscripts j, m, and n are the location index.

Apply the spatial discretization strategy mentioned above, and the discrete form of equation 3 for the scalar anomalous magnetic potential can be written as

$$U_a(x,y,z) = \sum_{n=1}^{N_z}\sum_{j=1}^{N_y}\sum_{i=1}^{N_x}\left(\int_{z_n-0.5\Delta z_n}^{z_n+0.5\Delta z_n}\int_{y_j-0.5\Delta y}^{y_j+0.5\Delta y}\int_{x_i-0.5\Delta x}^{x_i+0.5\Delta x} \times \mathbf{G}_U(x-x', y-y', z-z')\mathrm{d}x'\mathrm{d}y'\mathrm{d}z'\right) \cdot \mathbf{M}(x_i, y_j, z_n), \quad \text{(A-1)}$$

with the assumption that each prismatic voxel has homogeneous magnetization. In equation A-1,

$$\mathbf{G}_U(\mathbf{r}, \mathbf{r}') = -\nabla G(\mathbf{r}, \mathbf{r}') \quad \text{(A-2)}$$

denotes the gradient of the scalar Green's function G.

ANOMALOUS MAGNETIC FIELD IN THE FOURIER DOMAIN

Taking the 2D Fourier transform of equation A-1 in the observation space and rearranging the terms, the corresponding spectrum expression for the anomalous magnetic potential is obtained:

$$\bar{U}_a(k_x, k_y, z) = W(k_x, k_y)\sum_{n=1}^{N_z}[\mathbf{I}(k_x, k_y, z, z_n) \cdot \bar{\mathbf{M}}(k_x, k_y, z_n)], \quad \text{(A-3)}$$

where k_x and k_y are the wavenumber in the x- and y-directions. The terms $W(k_x, k_y)$ and $\bar{\mathbf{M}}(k_x, k_y, z_n)$ are given by

$$W(k_x,k_y)=\frac{4\sin(k_x\Delta x/2)\sin(k_y\Delta y/2)}{k_xk_y\Delta x\Delta y},$$

$$\bar{\mathbf{M}}(k_x,k_y,z_n)=\sum_{j=1}^{N_y}\sum_{i=1}^{N_x}\mathbf{M}(x_i,y_j,z_n)e^{-ik_xx_i}e^{-ik_yy_j}\Delta x\Delta y. \tag{A-4}$$

Obviously, $\bar{\mathbf{M}}$ has the same form of the expression for the 2D discrete Fourier transform of the magnetization. Hence, $\bar{\mathbf{M}}$ can be easily calculated by taking the 2D Fourier transform of $\mathbf{M}$.

In equation A-3, $\mathbf{I}$ is a single integral only related to the scalar Green's function and has the form of

$$\mathbf{I}(k_x,k_y,z,z_n)=\int_{z_n-0.5\Delta z_n}^{z_n+0.5\Delta z_n}\bar{\mathbf{G}}_U(k_x,k_y,z-z')\mathrm{d}z', \tag{A-5}$$

where $\bar{\mathbf{G}}_U(k_x,k_y,z-z')$ is the spectra of $\mathbf{G}_U(x,y,z-z')$. Using equation A-2 and the 2D Fourier transform given by Nabighian (1987), i.e.,

$$\int_{-\infty}^{\infty}\int_{-\infty}^{\infty}\frac{1}{4\pi\sqrt{x^2+y^2+(z-z')^2}}e^{-i(k_xx+k_yy)}\mathrm{d}x\mathrm{d}y=\frac{1}{2k}e^{-k|z-z'|},\quad\left(k=\sqrt{k_x^2+k_y^2}\right), \tag{A-6}$$

we obtain

$$\bar{\mathbf{G}}_U(k_x,k_y,z-z')=-\frac{1}{2k}e^{-k|z-z'|}(ik_x,ik_y,-\mathrm{sign}(z-z')\cdot k), \tag{A-7}$$

with

$$\mathrm{sign}(z-z')=\begin{cases}1, & z-z'>0\\ -1, & z-z'<0\end{cases}. \tag{A-8}$$

Then, the integral $\mathbf{I}$ can be conveniently calculated by substituting equation A-7 into equation A-5. We note that each prismatic voxel is regarded as an elementary source in this process. Therefore, for each prismatic voxel, the following three cases should be considered:

1) The observation point is above the prismatic voxel, i.e., $z>z'$,

$$\mathbf{I}(k_x,k_y,z,z_n)=\frac{e^{-kz}}{2k^2}e^{kz_n}(e^{-0.5k\Delta z_n}-e^{0.5k\Delta z_n})(ik_x,ik_y,-k). \tag{A-9}$$

2) The observation point is inside the prismatic voxel, i.e., $z_n-0.5\Delta z_n<z<z_n+0.5\Delta z_n$,

$$\mathbf{I}(k_x,k_y,z,z_n)=\frac{1}{2k^2}(e^{-kz}e^{kz_n}e^{-0.5k\Delta z_n}-1)(ik_x,ik_y,-k)+\frac{1}{2k^2}(e^{kz}e^{-kz_n}e^{-0.5k\Delta z_n}-1)(ik_x,ik_y,k). \tag{A-10}$$

3) The observation point is below the prismatic voxel, i.e., $z<z'$,

$$\mathbf{I}(k_x,k_y,z,z_n)=\frac{e^{kz}}{2k^2}e^{-kz_n}(e^{-0.5k\Delta z_n}-e^{0.5k\Delta z_n})(ik_x,ik_y,k). \tag{A-11}$$

Substituting equations A-9–A-11 into A-3 and rearranging the terms, $\bar{U}_a$ can be rewritten in a form with lots of merit in numerical calculation:

$$\begin{aligned}\bar{U}_a(k_x,k_y,z)=\frac{W(k_x,k_y)}{2k^2}\Bigg[&\sum_{n,z_n<z}A_1(k_x,k_y,z_n)K(k_x,k_y,z_n)\\&+\sum_{n,z_n=z}^{N_z}A_2(k_x,k_y,z_n)K(k_x,k_y,z_n)\\&+\sum_{n,z_n=z}^{N_z}A_2(k_x,k_y,z_n)F(k_x,k_y,z_n)\\&+\sum_{n,z_n<z}A_1(k_x,k_y,z_n)F(k_x,k_y,z_n)\\&-2\sum_{n,z_n=z}^{N_z}P(k_x,k_y,z_n)\Bigg],\end{aligned} \tag{A-12}$$

where

$$\begin{aligned}A_1(k_x,k_y,z_n)&=e^{-k|z-z_n|}(e^{-0.5k\Delta z_n}-e^{0.5k\Delta z_n}),\\A_2(k_x,k_y,z_n)&=e^{-k|z-z_n|}e^{-0.5k\Delta z_n},\\P(k_x,k_y,z_n)&=ik_x\bar{M}_x(k_x,k_y,z_n)+ik_y\bar{M}_y(k_x,k_y,z_n),\\F(k_x,k_y,z_n)&=P(k_x,k_y,z_n)+k\bar{M}_z(k_x,k_y,z_n),\\K(k_x,k_y,z_n)&=P(k_x,k_y,z_n)-k\bar{M}_z(k_x,k_y,z_n).\end{aligned} \tag{A-13}$$

Then, the anomalous magnetic field in the Fourier domain can be immediately obtained by

$$\begin{aligned}\bar{H}_{ax}(k_x,k_y,z)&=-ik_x\bar{U}_a(k_x,k_y,z),\\\bar{H}_{ay}(k_x,k_y,z)&=-ik_y\bar{U}_a(k_x,k_y,z),\\\bar{H}_{az}(k_x,k_y,z)&=-\frac{\mathrm{d}}{\mathrm{d}z}\bar{U}_a(k_x,k_y,z).\end{aligned} \tag{A-14}$$

Finally, the 2D inverse Fourier transforms of equation A-14 give $\mathbf{H}_a$ or $\mathbf{B}_a=\mu_0\mathbf{H}_a$, where μ_0 is the permeability of free space.

APPENDIX B
ANALYTICAL SOLUTIONS

Following the approach provided by Kaufman (1992), the anomalous magnetic field outside a magnetic sphere or spherical shell can be expressed as

$$\mathbf{H}_a = C_m \begin{bmatrix} 3(x-x_0)^2 - r^2 & 3(y-y_0)(x-x_0) & 3(z-z_0)(x-x_0) \\ 3(y-y_0)(x-x_0) & 3(y-y_0)^2 - r^2 & 3(z-z_0)(y-y_0) \\ 3(z-z_0)(x-x_0) & 3(z-z_0)(y-y_0) & 3(z-z_0)^2 - r \end{bmatrix} \mathbf{H}_0, \tag{B-1}$$

where $r = \sqrt{(x-x_0)^2 + (y-y_0)^2 + (z-z_0)^2}$ denotes the distance from the observation point (x, y, z) to the center of the magnetic body (x_0, y_0, z_0). The term $\mathbf{H}_0$ is the background magnetic field. For a magnetic sphere,

$$C_m = \frac{\chi}{3+\chi}\frac{r_0^3}{r^5}, \tag{B-2}$$

and for a magnetic spherical shell,

$$C_m = \frac{\chi(2\chi+3)(1-r_i^{-3}r_0^3)}{2\chi^2 - (2\chi+3)(3+\chi)r_i^{-3}r_0^3}\frac{r_0^3}{r^5}. \tag{B-3}$$

REFERENCES

Bhattacharyya, B. K., 1964, Magnetic anomalies due to prism-shaped bodies with arbitrary polarization: Geophysics, **29**, 517–531, doi: 10.1190/1.1439386.

Bhattacharyya, B. K., and K. C. Chan, 1977, Computation of gravity and magnetic anomalies due to inhomogeneous distribution of magnetization and density in a localized region: Geophysics, **42**, 602–609, doi: 10.1190/1.1440731.

Bhattacharyya, B. K., and M. E. Navolio, 1976, A fast Fourier transform method for rapid computation of gravity and magnetic anomalies due to arbitrary bodies: Geophysical Prospecting, **24**, 633–649, doi: 10.1111/j.1365-2478.1976.tb01562.x.

Billings, S. D., 2004, Discrimination and classification of buried unexploded ordnance using magnetometry: IEEE Transactions on Geoscience and Remote Sensing, **42**, 1241–1251, doi: 10.1109/TGRS.2004.826803.

Blakely, R. J., 1996, Potential theory in gravity and magnetic applications: Cambridge University Press.

Bott, M. H., 1963, Two methods applicable to computers for evaluating magnetic anomalies due to finite three-dimensional bodies: Geophysical Prospecting, **11**, 292–299, doi: 10.1111/j.1365-2478.1963.tb02039.x.

Boyd, J. P., T. Marilyn, and P. T. S. Eliot, 2001, Chebyshev and Fourier spectral methods: Dover Publications, U.S.

Butler, D. K., L. Pasion, S. Billings, D. Oldenburg, and D. Yule, 2003, Enhanced discrimination capability for UXO geophysical surveys, *in* R.S. Harmon, J. H. Holloway, and J.T. Broach, eds., Proceedings of SPIE Detection and Remediation Technologies and Mines and Minelike Targets VIII, 968–969.

Butler, D. K., P. J. Wolfe, and R. O. Hansen, 2001, Analytical modeling of magnetic and gravity signatures of unexploded ordnance: Journal of Environmental and Engineering Geophysics, **6**, 33–46, doi: 10.4133/JEEG6.1.33.

Chai, Y. P., and W. J. Hinze, 1988, Gravity inversion of an interface above which the density contrast varies exponentially with depth: Geophysics, **53**, 837–845, doi: 10.1190/1.1442518.

Chen, L. W., S. K. Dai, and M. P. Wu, 2016, Computation of discrete frequency when using FFT algorithm with random sampling points: Progress in Geophysics, **31**, 164–169.

Clark, D. A., S. J. Saul, and D.W. Emerson, 1986, Magnetic and gravity anomalies of a triaxial ellipsoid: Exploration Geophysics, **17**, 189–200, doi: 10.1071/EG986189.

Emerson, D. W., D. A. Clark, and S. J. Saul, 1985, Magnetic exploration models incorporating remanence, demagnetization and anisotropy: HP 41C handheld computer algorithms: Exploration Geophysics, **16**, 1–122, doi: 10.1071/EG985001.

Eskola, L., and T. Tervo, 1980, Solving the magnetostatic field problem (a case of high susceptibility) by means of the method of subsections: Geoexploration, **18**, 79–95, doi: 10.1016/0016-7142(80)90022-8.

Furness, P., 1999, A versatile integral equation technique for magnetic modeling: Journal of Applied Geophysics, **41**, 345–357, doi: 10.1016/S0926-9851(99)00005-1.

Gay, S. P., Jr., 1963, Standard curves for interpretation of magnetic anomalies over long tabular bodies: Geophysics, **28**, 161–200, doi: 10.1190/1.1439164.

Guo, W., M. Dentith, R. T. Bird, and D. A. Clark, 2001, Systematic error analysis of demagnetization and implications for magnetic interpretation: Geophysics, **66**, 562–570, doi: 10.1190/1.1444947.

Hjelt, S. E., 1972, Magnetostatic anomalies of dipping prisms: Geoexploration, **10**, 239–254.

Jackson, J. D., 1999, Classical electrodynamics, 3rd ed.: Hamilton Printing Company.

Jin, J., 2002, The finite element method in electromagnetics: Wiley.

Kaufman, A. A., 1992, Geophysical field theory and method part: Academic Press.

Ku, C. C., 1977, A direct computation of gravitational and magnetic anomalies caused by 2- and 3-dimensional bodies of arbitrary shape and arbitrary magnetic polarization by equivalent-point method and a simplified cubic spline: Geophysics, **42**, 610–622, doi: 10.1190/1.1440732.

Lee, T. J., 1980, Rapid computation of magnetic anomalies with demagnetization included, for arbitarily shaped magnetic bodies: Geophysical Journal of the Royal Astronomical Society, **60**, 67–75, doi: 10.1111/j.1365-246X.1980.tb02581.x.

Lelievre, P. G., and D. W. Oldenburg, 2006, Magnetic forward modeling and inversion for high susceptibility: Geophysical Journal International, **166**, 76–90, doi: 10.1111/j.1365-246X.2006.02964.x.

Nabighian, M. N., 1987, Electromagnetic methods in applied geophysics: Theory: SEG.

Phillips, H. B., 1934, Effect of surface discontinuity on the distribution of potential: Journal of Mathematical Physics, **13**, 261–267, doi: 10.1002/sapm1934131261.

Purss, M. B. J., and J. P. Cull, 2005, A new iterative method for computing the magnetic field at high magnetic susceptibilities: Geophysics, **70**, no. 5, L53–L62, doi: 10.1190/1.2052469.

Sanchez, V., Y. Li, M. N. Nabighian, and D. L. Wright, 2008, Numerical modeling of higher order magnetic moments in UXO discrimination: IEEE Transactions on Geoscience and Remote Sensing, **46**, 2568–2583, doi: 10.1109/TGRS.2008.918090.

Sharma, P. V., 1966, Rapid computation of magnetic anomalies and demagnetization effects caused by bodies of arbitrary shape: Pure and Applied Geophysics, **64**, 89–109, doi: 10.1007/BF00875535.

Sharma, P. V., 1968, Demagnetization effect of a rectangular prism: Geophysics, **33**, 132–134, doi: 10.1190/1.1439915.

Takahashi, D., and V. C. Oliveira Jr., 2017, Ellipsoids (v1.0): 3D magnetic modelling of ellipsoidal bodies: Geo-scientific Model Development Discussions, **10**, 1–28.

Talwani, M., 1965, Computation with the help of a digital computer of magnetic anomalies caused by bodies of arbitrary shape: Geophysics, **30**, 797–817, doi: 10.1190/1.1439654.

Telford, W. M., L. P. Geldart, and R. E. Sheriff, 1990, Applied geophysics: Cambridge University Press.

Tontini, F. C., L. Cocchi, and C. Carmisciano, 2009, Rapid 3-D forward model of potential fields with application to the Palinuro Seamount magnetic anomaly (southern Tyrrhenian Sea, Italy): Journal of Geophysical Research, **114**, B02103.

Wu, L. Y., 2016, Efficient modelling of gravity effects due to topographic masses using the Gauss-FFT method: Geophysical Journal International, **205**, 160–178, doi: 10.1093/gji/ggw010.

Wu, L. Y., and L. W. Chen, 2016, Fourier forward modeling of vector and tensor gravity fields due to prismatic bodies with variable density contrast: Geophysics, **81**, no. 1, G13–G26, doi: 10.1190/geo2014-0559.1.

Wu, L. Y., and G. Tian, 2014, High-precision Fourier forward modeling of potential fields: Geophysics, **79**, no. 5, G59–G68, doi: 10.1190/geo2014-0039.1.

Zhang, Y., L. Collins, H. Yu, C. E. Baum, and L. Carin, 2003, Sensing of unexploded ordnance with magnetometer and induction data — Theory and signal processing: IEEE Transactions on Geoscience and Remote Sensing, **41**, 1005–1015, doi: 10.1109/TGRS.2003.810922.

Zhao, G., B. Chen, L. Chen, J. Liu, and Z. Ren, 2018, High-accuracy 2D and 3D Fourier forward modeling of gravity field based on the Gauss-FFT method: Journal of Applied Geophysics, **150**, 294–303, doi: 10.1016/j.jappgeo.2018.01.002.

Zhdanov, M. S., and S. Fang, 1997, Quasi-linear series in three-dimensional electromagnetic modeling: Radio Science, **32**, 2167–2188, doi: 10.1029/97RS02284.